

Article

Layered Acoustic Structures with Equally Phased Elements

Paola Gori ^{1,*}, Claudia Guattari ², Luca Evangelisti ¹, Roberto De Lieto Vollaro ¹ and Francesco Asdrubali ³

¹ Department of Industrial, Electronic and Mechanical Engineering, Roma Tre University, Via della Vasca Navale 79, 00146 Rome, Italy; luca.evangelisti@uniroma3.it (L.E.); roberto.delietovollaro@uniroma3.it (R.D.L.V.)

² Department of Philosophy, Communication and Performing Arts, Roma Tre University, Via Ostiense 139, 00154 Rome, Italy; claudia.guattari@uniroma3.it

³ Department of International Human and Social Sciences, Perugia Foreigners' University, Piazza Fortebraccio 4, 06122 Perugia, Italy; francesco.asdrubali@unistrapg.it

* Correspondence: paola.gori@uniroma3.it

Abstract: It is often required to control the acoustic transmission across layered structures in order to favor or, more frequently, limit it in prescribed energy ranges. The selection of the materials and layer thicknesses needed to achieve a given objective is not straightforward, and it is often performed empirically. This is connected with the lack of simple models that dictate the frequency behavior of the layered structure. In this work, we present an approach to the systematic design of layered media, based on an assumption that allows us to obtain simple analytical expressions for the occurrence of bandgaps in the frequency response of ideally infinite periodic structures. Correspondingly low-transmission frequency ranges are then analyzed and discussed in finite-thickness realizations of the designed periodic structures.

Keywords: layered structures; transfer matrix method; transmission function; bandgap; periodic crystals; unit cell



Academic Editor: Jian Kang

Received: 16 January 2025

Revised: 19 February 2025

Accepted: 28 February 2025

Published: 4 March 2025

Citation: Gori, P.; Guattari, C.; Evangelisti, L.; De Lieto Vollaro, R.; Asdrubali, F. Layered Acoustic Structures with Equally Phased Elements. *Acoustics* **2025**, *7*, 12. <https://doi.org/10.3390/acoustics7010012>

Copyright: © 2025 by the authors. Licensee MDPI, Basel, Switzerland. This article is an open access article distributed under the terms and conditions of the Creative Commons Attribution (CC BY) license (<https://creativecommons.org/licenses/by/4.0/>).

1. Introduction

Layered structures are frequently occurring or are purposely designed in acoustics, ultrasonics as well as in other wave domains [1–4]. The interest lies in the fact that the interference between the waves that cross a layered structure gives rise to a frequency behavior of the transmission function that varies significantly depending on the materials and thicknesses of the layers. Methods to tailor such frequency response to the specific application are therefore needed. Once such a method is available, there are powerful tools, such as 3D printing [5–7], that can be used to realize a structure whose effectiveness relies on the careful realization of its theoretically engineered design. Layering is the simplest approach to tune the properties of a structure, but its design is often done empirically or numerically [8–11] because of the lack of models dictating the frequency behavior that are simple enough to be used for an analytic description.

To deal with stratified media or layered structures, a one-dimensional model can be built, where each single layer is assumed to be a homogeneous, lossless medium [12]. The propagation problem can be treated with several approaches, such as plane wave expansion, multiple scattering, or finite-element methods [13]. Here we shall use the transfer matrix method [14], which is a simple and powerful tool. The transfer matrix method is often used not only in acoustics [13,15,16], but also in electromagnetism [17,18], in seismology [19,20], in quantum mechanics [21,22], because in all cases a similar wave description of the physical phenomenon applies. In acoustics, the transfer matrix method is also employed when

dealing with porous media where the material is not strictly homogeneous but it can be described by means of effective, frequency-dependent, density and compressibility [23,24]. A multilayer structure, including porous layers or not, can be studied by multiplying the transfer matrices pertaining to each component [25]. Although the formal description of the propagation in a layered medium is therefore simple, the analytic expressions of the elements of the overall matrix increase rapidly their complexity with the number of layers. Therefore, a synthesis that aims at obtaining, for example, a small transmission in a given frequency range is not trivial and usually requires a trial-and-error approach.

In this work, we address the design of layered acoustic structures in the framework of periodic 1D systems. The infinite repetition of a unit cell gives rise to a number of bandgaps, i.e., frequency ranges for which the transmission across the periodic structure is forbidden. This imposed artificial periodicity makes layered structures the simplest type of phononic, or sonic, crystal [26–30]. The locations and widths of the bandgaps depend on the thicknesses and impedances of the constitutive layers in the unit cell. This dependence is in general not known through analytic expressions. However, we show that, by introducing a simplifying assumption on the materials and/or thicknesses of the component layers, a simple description of the frequency response of the structure can be found. This proves to be extremely useful both if one deals with an analysis problem or a synthesis problem. While in the first case there is a clear and direct route from a model to its application and solution, a synthesis problem, which consists in devising a way to achieve prescribed performances, is more elusive, as there may be different approaches to reach the objective, and it can also happen that no solution is available within given constraints. The approach proposed here is based on the assumption of a Goupillaud-type layered medium, a model that is used in geophysics [31–33] and in the propagation of acoustic waves in air/water mixtures [34].

Within this assumption, which we define the ‘cophasal hypothesis’, we will show that it is possible to analytically derive the dispersion relation for infinite crystals, and we will explicitly analyze the cases with two to five layers per unit cell. The knowledge of the dispersion relation will allow us to determine the locations and widths of the bandgaps, whose expressions will be easily obtained by resorting to the solution of second-degree equations. For crystals with six to nine layers per cell, analytical expressions can be determined anyway, although they become more cumbersome. In any case, periodic structures requiring a unit cell with more than few units would be not very practical to realize.

The issue of the approximation of the periodic crystal by means of a finite number of cells will be then addressed. The process leading to the formation of bandgaps, or, more precisely, to low-transmission frequency ranges, will be illustrated, by highlighting the role played by the number of unit cells employed and by the impedance mismatch between the layers. In particular, in the case of a two-layer unit cell, the value of the modulus of the transmission function at the middle of the Irreducible Brillouin Zone (IBZ) [1], around which a bandgap is located for the infinite crystal, will be analytically derived. This value comes out to be monotonically decreasing with increasing number of cells of the finite crystal and can be therefore used to calculate the number of cells needed to achieve a prescribed value of the modulus of the transmission function at the middle of the IBZ. A few properties of finite crystals with three or more layers per cell will be finally illustrated.

The method proposed here aims at facilitating the design of layered structures, to be used in the acoustic or ultrasonic range, through the application of simple analytic relationships for the location and width of bandgaps. The specific problems where this approach can prove useful dictate the constraints on the materials to employ, including innovative and sustainable ones [35,36], and on the layer thicknesses.

The paper is structured as follows. After recalling the basic formalism used to address the problem in Section 2, in Section 3 we apply the cophasal assumption to derive the dispersion law in ideal infinite crystals (Section 3.1) with two to five layers per cell, mentioning also what happens for a higher number of layers. Then, in Section 3.2, we address the issue of the transmission properties of finite crystals, arising from the repetition of a finite number of cells, and compare their behavior with that of the corresponding infinite structure.

2. Materials and Methods

2.1. Preliminaries

With reference to a typical situation, we consider the case of an acoustic wave propagating along the positive direction of the z -axis of a suitable reference. We assume the wave to be purely longitudinal, as it happens in an inviscid fluid. In addition, the medium characteristic impedance is taken to be a piece-wise constant function of z only, with the wave impinging normally on the boundary between two different media.

Across a typical $z = \text{constant}$ plane, the wave is specified by the pressure p and the normal particle velocity v it produces along the z -axis. These quantities can be used to specify a state vector represented by a column vector as follows

$$\mathbf{u} = \begin{bmatrix} p \\ v \end{bmatrix}. \quad (1)$$

Consider two planes orthogonal to the z -axis, one located at $z = 0$ and the other at $z = a$, and assume the medium between them is acted upon by a harmonic plane wave. On imposing the boundary conditions on the two planes for pressure and normal particle velocity, it is found [13] that the state vectors at the entrance and exit plane are connected by the relation (with obvious notations)

$$\begin{bmatrix} p_0 \\ v_0 \end{bmatrix} = \begin{bmatrix} \cos(ka) & iZ \sin(ka) \\ \frac{i}{Z} \sin(ka) & \cos(ka) \end{bmatrix} \begin{bmatrix} p \\ v \end{bmatrix}, \quad (2)$$

which can be briefly expressed as

$$\mathbf{u}_0 = \mathbf{T} \mathbf{u}, \quad (3)$$

where \mathbf{u}_0 and \mathbf{u} denote the entrance and exit state vectors, respectively, and \mathbf{T} is the transfer matrix. The quantities k , a , and Z denote the wavenumber, the layer thickness, and the characteristic impedance, respectively, Z being connected to the density ρ and the sound speed c pertaining to the layer by $Z = \rho c$ [37].

2.2. Dispersion Law

We start from basic concepts related to the dispersion law of a multilayer structure obtained by the repetition of a unit cell (see Figure 1 for a sketch of the geometry of the problem). Let us begin with known results of a sequence where the unit cell is obtained by cascading N layers with transfer matrices

$$\mathbf{T}_s = \begin{bmatrix} \cos(k_s a_s) & iZ_s \sin(k_s a_s) \\ \frac{i}{Z_s} \sin(k_s a_s) & \cos(k_s a_s) \end{bmatrix}, \quad (s = 1, 2, \dots, N), \quad (4)$$

where the subscript s indicates that all the quantities are specific of the s -th layer. The transfer matrix of the unit cell is given by the product

$$\mathbf{T} = \mathbf{T}_1 \mathbf{T}_2 \dots \mathbf{T}_N. \quad (5)$$

Note that the arguments of the sinusoidal functions appearing in \mathbf{T}_s in Equation (4) depend on the product of the wavenumber times the layer thickness. Then, layers with different material properties can give rise to the same phase value if the thicknesses are properly chosen. When this is done, we shall speak of equally phased (or cophasal, for brevity) layers. This means that the layers have, individually, the same natural frequencies, which are, in turn, a subset of those of the whole structure. The pertaining transfer matrices will be different from each other, though, because we shall assume the impedance of the layers' materials to be different (otherwise the elements would collapse into a single one). The cophasal layers assumption is equivalent to having a Goupillaud-type layered medium [31], defined by the requirement that the wave has the same travel time through each layer. Even if restrictive, this hypothesis has the advantage of allowing us to get closed-form results, which will constitute a reference case also when the hypothesis applies only approximately.

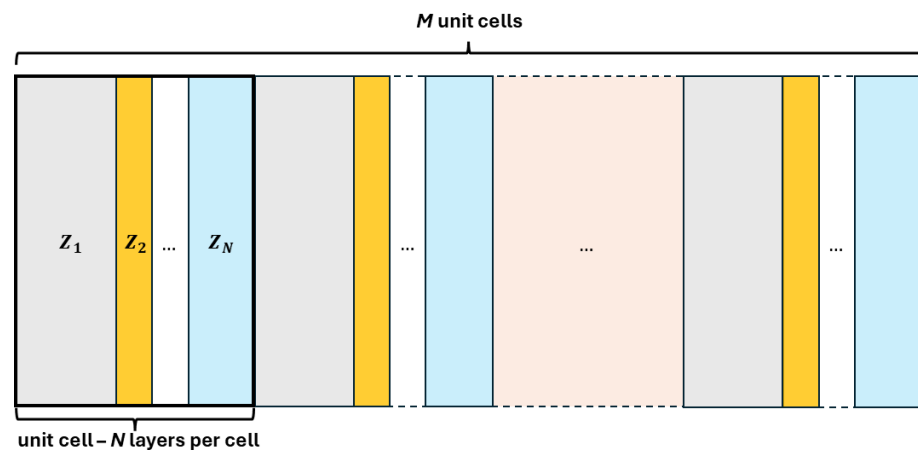


Figure 1. Schematic geometry of the addressed problem: a unit cell composed by N layers with different characteristic impedances, $Z_i, i = 1, \dots, N$, is repeated an infinite number of times, in the case of an ideal crystal or, in a finite approximation of it, M times, as indicated in the figure.

From now on, therefore, we shall adopt the hypothesis of dealing with a unit cell made of cophasal layers and we will call the equal phases

$$\gamma = k_1 a_1 = k_2 a_2 = \dots = k_N a_N. \quad (6)$$

The half sum of the diagonal elements of the overall matrix \mathbf{T} can be set equal to the cosine of an equivalent wavenumber k_e times the overall cell length [13]

$$a = \sum_{s=1}^N a_s. \quad (7)$$

The presumption of representing the multilayer structure by means of an equivalent homogeneous medium may lead to apparently meaningless results, when $|\cos(k_e a)| > 1$, but it is precisely in this way that, by accepting complex values for the cosine, the occurrence of bandgaps can be introduced.

Before starting analyzing unit cells with a progressively increased number of layers, we observe that, in the particular case of N equal layers, the medium is actually homogeneous and the dispersion relation is obtained as

$$\cos(k_e a) = \cos(N\gamma) = T_N(\cos \gamma) = \sum_{m=0}^{[N/2]} (-1)^m \binom{N}{2m} \cos \gamma^{N-2m} \sin \gamma^{2m}, \quad (8)$$

where T_N denotes the N -th Chebishev polynomial of the first kind and order N [38], and the square brackets stand for integer part.

3. Results

3.1. Infinite Crystals

3.1.1. Two Layers per Cell

Adopting the cophasal hypothesis, in the case of two layers per cell Equations (4) and (5) give

$$\begin{aligned} \mathbf{T} &= \begin{bmatrix} \cos \gamma & iZ_1 \sin \gamma \\ \frac{i}{Z_1} \sin \gamma & \cos \gamma \end{bmatrix} \begin{bmatrix} \cos \gamma & iZ_2 \sin \gamma \\ \frac{i}{Z_2} \sin \gamma & \cos \gamma \end{bmatrix} \\ &= \begin{bmatrix} \cos^2 \gamma - \frac{Z_1}{Z_2} \sin^2 \gamma & i(Z_1 + Z_2) \sin \gamma \cos \gamma \\ i\left(\frac{1}{Z_1} + \frac{1}{Z_2}\right) \sin \gamma \cos \gamma & \cos^2 \gamma - \frac{Z_2}{Z_1} \sin^2 \gamma \end{bmatrix} \end{aligned} \quad (9)$$

From the half sum of the diagonal elements of the overall matrix in Equation (9), the dispersion relation is obtained as

$$\cos(k_e a) = \cos^2 \gamma - K_2 \sin^2 \gamma, \quad (10)$$

in which we introduced the notation

$$K_2 = \frac{1}{2} \left[\frac{Z_1}{Z_2} + \frac{Z_2}{Z_1} \right], \quad (11)$$

where the index of K , to be shortly generalized, refers to the number of layers of the cell. We can call K_2 a mismatch parameter. Here and in the following, we will always have to do with impedance ratios and, therefore, we shall be allowed to use pure numbers in the numerical examples.

Note that, being a function of $\cos^2 \gamma$, the product of the equivalent wavenumber k_e times the cell length a has period π . We also remark that, for $x > 0$, the function $(x + 1/x)/2$ has a minimum equal to 1 for $x = 1$. Then, except for $Z_1 = Z_2$, K_2 is greater than one, and hence $\cos(k_e a)$ can become smaller than -1 . A few examples can be seen in Figure 2a, where, in addition to the curve corresponding to $K_2 = 1.0$, the cases $K_2 = 1.5, 3.0, 6.0, 20$, with decreasing minima, are shown. The horizontal line with -1 ordinate is also plotted for comparison. For values smaller than -1 , the arccos function has no meaning in the real realm and takes on complex values. The interval of γ values where this occurs is called a bandgap [13] because only evanescent waves can exist in it. Such an interval is limited by the solutions of the equation obtained by imposing the r.h.s of Equation (10), let us call it $D_2(\gamma)$,

$$D_2(\gamma) = \cos^2 \gamma - K_2 \sin^2 \gamma, \quad (12)$$

to be equal to -1 , which gives

$$(1 + K_2) \cos^2 \gamma - K_2 = -1. \tag{13}$$

The width of the bandgap, say $\Delta\gamma$, is therefore

$$\Delta\gamma = \arccos\left(-\sqrt{\frac{K_2 - 1}{K_2 + 1}}\right) - \arccos\left(\sqrt{\frac{K_2 - 1}{K_2 + 1}}\right) = \pi - 2 \arccos\left(\sqrt{\frac{K_2 - 1}{K_2 + 1}}\right). \tag{14}$$

$\Delta\gamma$ is equal to the interval between the two crossings of the horizontal dashed line denoting -1 ordinate in Figure 2a. Equation (14) shows that these crossings always exist as soon as $K_2 > 1$. The relative bandgap $\Delta\gamma/\pi$ amounts, respectively, to 0.00, 0.30, 0.50, 0.64, 0.80 for the values of K_2 reported in Figure 2. It is seen that, on increasing K_2 , the bandgap gets larger and larger tending to occupy a major part of the interval $(0, \pi)$. If the two layers in the unit cell are air and water, for example, $K_2 = 1.8 \cdot 10^3$ and $\Delta\gamma/\pi = 0.98$, i.e., the allowed bands are extremely small.

The width $\Delta\gamma$ of the bandgap as a function of K_2 is drawn in Figure 3. A Taylor expansion of the arccos functions around zero gives the approximate bandwidth expression

$$\Delta\gamma \simeq 2\sqrt{\frac{K_2 - 1}{K_2 + 1}}, \tag{15}$$

that applies when the impedances of the two layers in the unit cell are not very different.

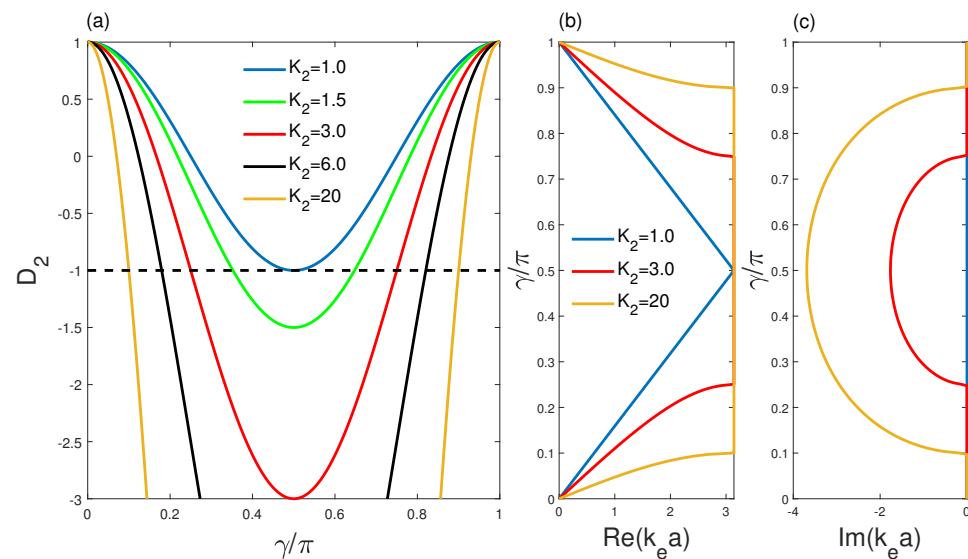


Figure 2. Crystal with two layers per cell. (a) Plots of the function $D_2(\gamma)$, defined in Equation (12), for the values shown of the parameter K_2 . Dispersion curves as functions of (b) the real part and (c) the imaginary part of $k_e a$ for $K_2 = 1.0$ (blue lines), $K_2 = 3.0$ (red lines) and $K_2 = 20$ (orange lines).

In Figure 2b,c, γ is plotted versus the real and imaginary parts of $k_e a$ for three values of K_2 . The triangular line corresponds to the minimum value, i.e., 1, of K_2 , for which only homogeneous waves are present (there are no bandgaps) and a linear relationship between k_e and γ occurs: in the IBZ, $\gamma = k_e a/2$ and $\gamma = \pi - k_e a/2$ (see Equation (10)). The red curve, corresponding to $K_2 = 3.0$, describes a dispersion regime in which γ exhibits a non-linear dependence on the real part of $k_e a$. When $\text{Re}(k_e a)$ reaches π (at the boundary of the first Brillouin zone) the transition occurs to the bandgap state. At this point one has to switch to Figure 2c where the imaginary k_e indicates the existence of an evanescent wave in the band gap. The extent of the vertical segment between the two red curves in Figure 2b

specifies the width of the bandgap. Similar features are shown for the case $K_2 = 20$, whose representative curves are plotted in orange. For both $K_2 = 3$ and $K_2 = 20$, one bandgap only exists within a period, as already indicated by Figure 2a.

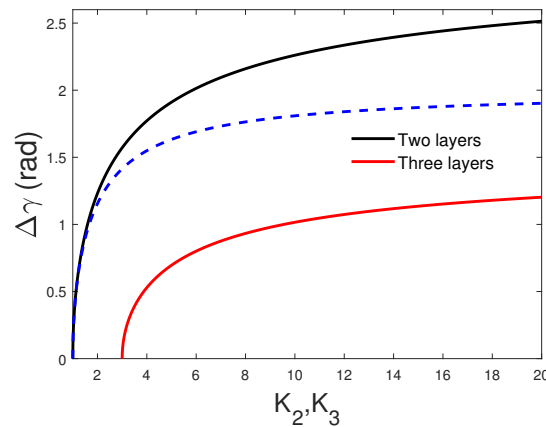


Figure 3. Width $\Delta\gamma$ of the bandgap as a function of K_2 (black line), for the case of two-layer cell, or K_3 (red line) for the case of three-layer cell. The blue dashed line represents the approximate expression in Equation (15) for the two-layer cell.

3.1.2. Three Layers per Cell

Let us move on to the case of three cophasal elements per cell. Proceeding as in the case of two layers, three 2×2 matrices are multiplied, and half the sum of the diagonal elements of the resulting matrix is taken as cosine of the new equivalent wavenumber times the overall layer thickness, which is again denoted by a . After simplification, the following relation is found

$$\cos(k_e a) = D_3(\gamma), \quad (16)$$

where

$$D_3(\gamma) = \cos^3 \gamma - K_3 \cos \gamma \sin^2 \gamma, \quad (17)$$

which has the same structure of Equation (12) multiplied by $\cos \gamma$. The mismatch parameter K_3 though differs from K_2 and has the following expression

$$K_3 = \frac{1}{2} \left\{ \left[\frac{Z_1}{Z_2} + \frac{Z_2}{Z_1} \right] + \left[\frac{Z_1}{Z_3} + \frac{Z_3}{Z_1} \right] + \left[\frac{Z_2}{Z_3} + \frac{Z_3}{Z_2} \right] \right\}. \quad (18)$$

The square brackets are used to put into evidence the three groups that appear in Equation (18) and have the same form as that of Equation (11). The minimum value of K_3 , which is reached when $Z_1 = Z_2 = Z_3$, regardless of their common value, is equal to 3. The order of magnitude of K_3 is roughly given by the ratio between the largest and the smallest of the three impedances. Notice that the expression of K_3 extends the formula given by Equation (11) to the case of three layers. It is remarkable that the dispersion relation depends on the single parameter K_3 although the physical structure depends on the three independent parameters Z_1, Z_2, Z_3 . Thus, there are infinitely many $(Z_i, i = 1, 2, 3)$ parameters producing the same dispersion relation except for the minimum value, namely 3, of K_3 . This first implies that the three impedances commute with each other, or, concretely, that the positions of two layers can be interchanged (although it can be easily shown that this, in general, would give rise to a different transmission function for a finite-length approximation of the ideal crystal). What is more significant is that the value of one of the impedances can be changed leaving unchanged the value of K_3 , and therefore the resulting dispersion law of the crystal, provided that another impedance is suitably changed, too. To determine how such a compensation has to be made, note that one of the impedances, say

Z_1 can be assumed to be one, as K_3 depends only on the ratios of impedances. Doing so, the expression of K_3 can be written

$$K_3 = \frac{1}{2} \left\{ \left[\frac{1}{Z_2} + Z_2 \right] + \left[\frac{1}{Z_3} + Z_3 \right] + \left[\frac{Z_2}{Z_3} + \frac{Z_3}{Z_2} \right] \right\}, \tag{19}$$

and this is a two-dimensional function describing the surface that appears as in Figure 4a. The function value remains constant along any curve that represents a contour line, with the shapes shown in Figure 4b.

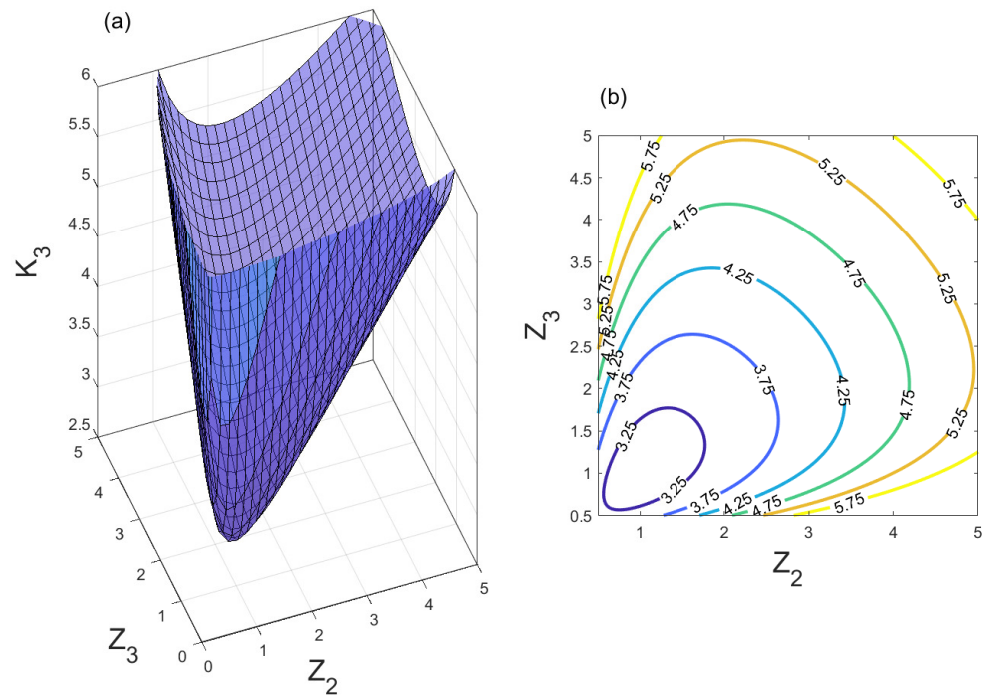


Figure 4. (a) Three-dimensional view of the surface identified by the function in Equation (19), which gives the parameter K_3 as a function of two (Z_2, Z_3) of the three impedances, with the third impedance (Z_1) being taken as one. (b) Contour lines of the same function.

Note that the path along which Z_2 and Z_3 have to change simultaneously to obtain a given K_3 has a length depending on the value of K_3 . When such a value nears the bottom of the surface K_3 , the range of possible changes of the pair (Z_2, Z_3) is progressively reduced.

Let us now examine in some more details the behavior of the function $D_3(\gamma)$ in Equation (17). A few plots of it are shown in Figure 5a for $K_3 = 3.0, 9.0, 20$. The horizontal lines corresponding to the ± 1 ordinates help visualizing the appearance of bandgaps when K_3 exceeds 3. Two bandgaps are now present. Notice that the width of the allowed bands decreases on increasing K_3 . This is particularly evident for the band centered at $\pi/2$.

While for the case of two layers the dispersion formula does not exceed 1, now there is no such limitation. We then have to find the values of γ for which the dispersion law equals 1 as well as those for which it equals -1 . To evaluate the thickness of the allowed and forbidden bands, the intersection points between the horizontal lines $z = \pm 1$ and the plots of the function $D_3(\gamma)$ in Equation (17) are to be found. This amounts to finding the roots of the following equations

$$\cos^3 \gamma - K_3 \cos \gamma \sin^2 \gamma = 1, \tag{20}$$

$$\cos^3 \gamma - K_3 \cos \gamma \sin^2 \gamma = -1. \tag{21}$$

The values $\cos \gamma = 1$ and $\cos \gamma = -1$ are at once seen to be solutions of Equations (20) and (21), respectively. Then, on dividing the r. h. sides of the equations by $\cos \gamma - 1$ and $\cos \gamma + 1$, respectively, two second degree equations remain. This behavior actually occurs in any case in which the number of layers per cell is odd: the equations that arise by imposing the crossing of the horizontal lines $z = \pm 1$ have the solutions $\cos \gamma = \pm 1$ and therefore the order of the equation is reduced by one on dividing it by $\cos \gamma \mp 1$. In the present case, the three solutions are

$$\begin{aligned} \cos \gamma &= 1, \\ \cos \gamma &= -\frac{1}{2} \pm \sqrt{\frac{1}{4} - \frac{1}{1 + K_3}}, \end{aligned} \tag{22}$$

for Equation (20) and

$$\begin{aligned} \cos \gamma &= -1, \\ \cos \gamma &= \frac{1}{2} \pm \sqrt{\frac{1}{4} - \frac{1}{1 + K_3}}, \end{aligned} \tag{23}$$

for Equation (21), respectively. While the two solutions $\cos \gamma = \pm 1$, and therefore $\gamma = 0, \pi$ in the IBZ, do not correspond to crossings of the horizontal lines $z = \pm 1$ and do not delimit bandgaps, the other four solutions in Equations (22) and (23), which are always real since $K_3 \geq 3$, can be used to determine the bandgap widths. This is shown for the first bandgap in Figure 3 as a function of K_3 . The second bandgap has the same width, as is easily understood from Figure 5a. As in the case of two layers per cell, the bandgap width increases with the mismatch parameter, here K_3 , but, since now the gaps are two equal ones, for each of them the width tends to a smaller value for large K_3 : $\Delta\gamma \rightarrow \pi/2$. For the values $K_3 = 9.0$ and 20 , that have been used in Figure 5a, the application of Equations (22) and (23) gives $\Delta\gamma/\pi = 0.31$ and 0.38 , respectively. In Figure 5b,c the dispersion curves are plotted versus the real and imaginary parts of $k_e a$ for the same three values of K_3 used in Figure 5a. When K_3 has the minimum value of 3 there is no bandgap and, as in the two layers per cell case, the relationship between γ and $k_e a$ is linear.

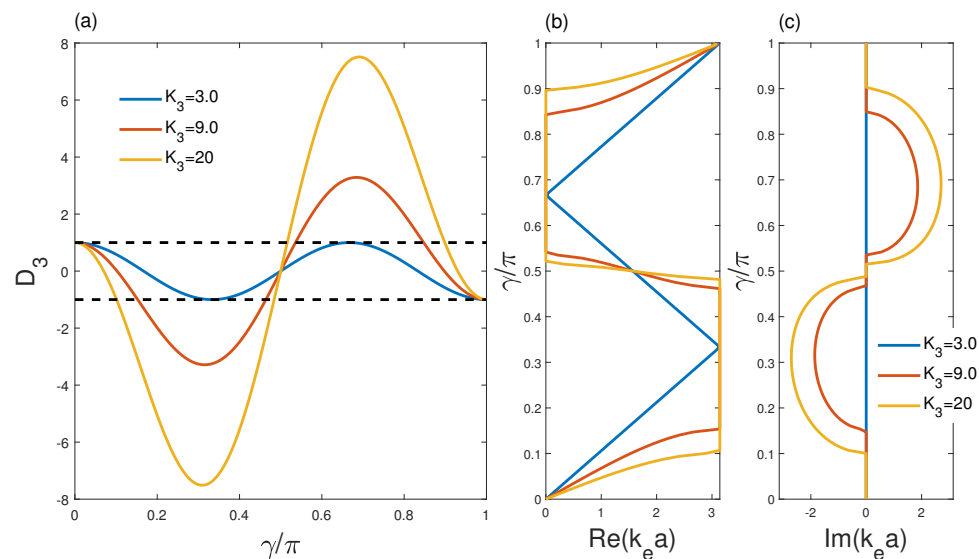


Figure 5. Crystal with three layers per cell. (a) Plots of the function $D_3(\gamma)$, defined in Equation (17), for three values of K_3 . Dispersion curves as functions of the (b) real part and (c) imaginary part of $k_e a$, plotted for the same values of K_3 .

3.1.3. Four Layers per Cell

We can now deal with the case of four elements per cell. Proceeding as in the previous cases, we have now to multiply four matrices. The dispersion law becomes

$$\cos(k_e a) = D_4(\gamma), \tag{24}$$

where

$$D_4(\gamma) = \cos^4 \gamma - K_4 \cos^2 \gamma \sin^2 \gamma + A_4 \sin^4 \gamma, \tag{25}$$

$$A_4 = \frac{1}{2} \left[\frac{Z_1 Z_3}{Z_2 Z_4} + \frac{Z_2 Z_4}{Z_1 Z_3} \right], \tag{26}$$

and

$$K_4 = \frac{1}{2} \left\{ \left[\frac{Z_1}{Z_2} + \frac{Z_2}{Z_1} \right] + \left[\frac{Z_1}{Z_3} + \frac{Z_3}{Z_1} \right] + \left[\frac{Z_1}{Z_4} + \frac{Z_4}{Z_1} \right] + \left[\frac{Z_2}{Z_3} + \frac{Z_3}{Z_2} \right] + \left[\frac{Z_2}{Z_4} + \frac{Z_4}{Z_2} \right] + \left[\frac{Z_3}{Z_4} + \frac{Z_4}{Z_3} \right] \right\}. \tag{27}$$

The minima of A_4 and K_4 , reached for $Z_1 = Z_2 = Z_3 = Z_4$, are equal to 1 and 6, respectively.

The parameters A_4 and K_4 are plotted in Figure 6 as functions of Z_2 and Z_3 (for fixed values of Z_1 and Z_4). A given value of each of the parameters is obtained when changing Z_2 and Z_3 according to the corresponding contour line. This does not mean, of course, that the same dispersion would be obtained when changing in this way the impedances, as both A_4 and K_4 would need to be constant to that aim.

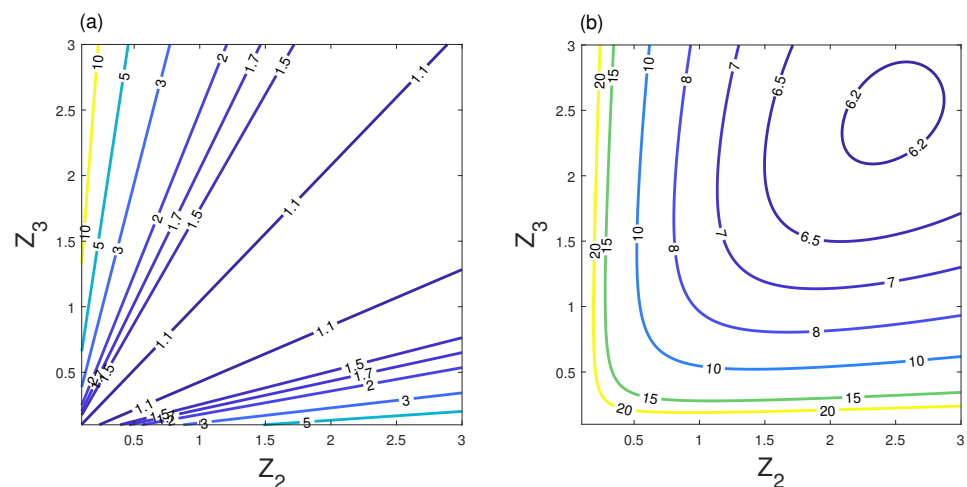


Figure 6. Four layers per cell. Contour plots of the parameters (a) A_4 and (b) K_4 vs. Z_2 and Z_3 , with $Z_1 = 3.0$ and $Z_4 = 2.0$.

The intersections between the dispersion curve and the line $\cos(k_e a) = 1$ are determined by solving the second degree equation

$$\cos^4 \gamma - K_4 \cos^2 \gamma (1 - \cos^2 \gamma) + A_4 (1 - \cos^2 \gamma)^2 = 1, \tag{28}$$

which gives the following roots

$$\begin{aligned} \cos \gamma &= \pm 1, \\ \cos \gamma &= \pm \frac{\sqrt{-1 + A_4}}{\sqrt{1 + A_4 + K_4}}. \end{aligned} \tag{29}$$

Being $A_4 \geq 1$, the roots are always real.

Similarly, the equation

$$\cos^4 \gamma - K_4 \cos^2 \gamma (1 - \cos^2 \gamma) + A_4 (1 - \cos^2 \gamma)^2 = -1, \tag{30}$$

has the roots

$$\cos \gamma = \pm \frac{1}{\sqrt{2}} \sqrt{\frac{2A_4 + K_4}{1 + A_4 + K_4} \pm \frac{\sqrt{K_4^2 - 4(1 + 2A_4 + K_4)}}{1 + A_4 + K_4}}. \tag{31}$$

Also in this case it may be verified that, given the limitations $K_4 \geq 6$ and $A_4 \geq 1$, the roots are always real. In particular, if three out of four impedances are equal, it is easy to show that the argument of the inner square root in Equation (31) is always positive and all four roots are real.

An example of dispersion, in the general case of four different media, is reported in Figure 7. Three bandgaps are shown to appear.

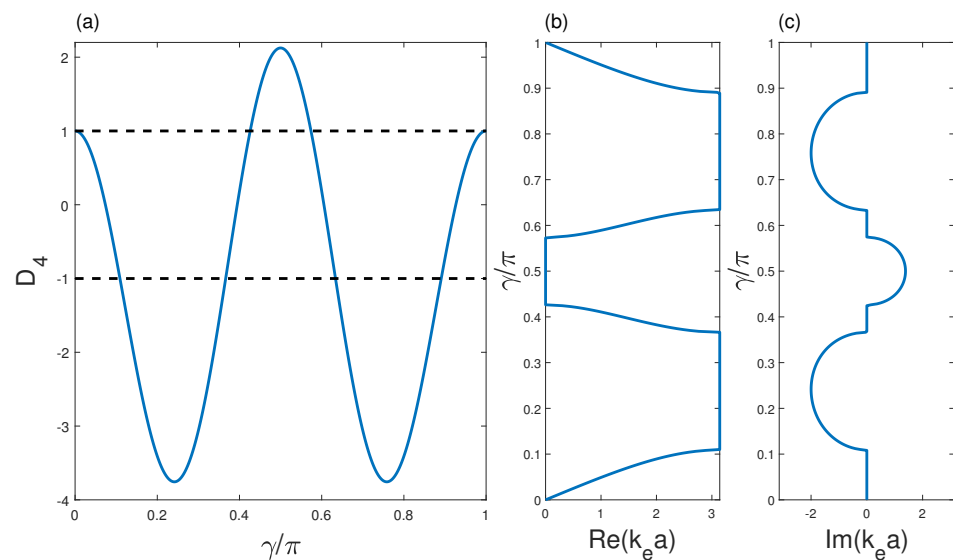


Figure 7. Crystal with four layers per cell. (a) Plot of the function $D_4(\gamma)$, defined in Equation (25), for $Z_1 = 7.0, Z_2 = 3.5, Z_3 = 0.5, Z_4 = 4.0$, giving $A_4 = 2.13$, and $K_4 = 18.1$. The horizontal lines $z = \pm 1$ point out the abscissas where $\cos(k_e a)$ goes above 1 or below -1 . Dispersion curves as functions of the real part (b) and imaginary part (c) of $k_e a$, plotted for the same values of A_4 and K_4 .

3.1.4. Five Layers per Cell

When there are five layers per unit cell, the dispersion relation reads

$$\cos(k_e a) = D_5(\gamma) \tag{32}$$

with

$$D_5(\gamma) = \cos^5 \gamma - K_5 \cos^3 \gamma \sin^2 \gamma + A_5 \cos \gamma \sin^4 \gamma \tag{33}$$

and where the constants A_5 and K_5 can be computed by means of the formulas

$$A_5 = \frac{1}{2} \left\{ \left[\frac{Z_1 Z_3}{Z_2 Z_4} + \frac{Z_2 Z_4}{Z_1 Z_3} \right] + \left[\frac{Z_1 Z_3}{Z_2 Z_5} + \frac{Z_2 Z_5}{Z_1 Z_3} \right] + \left[\frac{Z_1 Z_4}{Z_2 Z_5} + \frac{Z_2 Z_5}{Z_1 Z_4} \right] + \left[\frac{Z_1 Z_4}{Z_3 Z_5} + \frac{Z_3 Z_5}{Z_1 Z_4} \right] + \left[\frac{Z_2 Z_4}{Z_3 Z_5} + \frac{Z_3 Z_5}{Z_2 Z_4} \right] \right\}, \tag{34}$$

and

$$K_5 = \frac{1}{2} \left\{ \left[\frac{Z_1}{Z_2} + \frac{Z_2}{Z_1} \right] + \left[\frac{Z_1}{Z_3} + \frac{Z_3}{Z_1} \right] + \left[\frac{Z_1}{Z_4} + \frac{Z_4}{Z_1} \right] + \left[\frac{Z_1}{Z_5} + \frac{Z_5}{Z_1} \right] + \left[\frac{Z_2}{Z_3} + \frac{Z_3}{Z_2} \right] + \left[\frac{Z_2}{Z_4} + \frac{Z_4}{Z_2} \right] + \left[\frac{Z_2}{Z_5} + \frac{Z_5}{Z_2} \right] + \left[\frac{Z_3}{Z_4} + \frac{Z_4}{Z_3} \right] + \left[\frac{Z_3}{Z_5} + \frac{Z_5}{Z_3} \right] + \left[\frac{Z_4}{Z_5} + \frac{Z_5}{Z_4} \right] \right\}, \quad (35)$$

respectively. As anticipated, when the number of layers per cell is odd, the degree of the equation to be solved for finding the boundaries of the bandgaps, now obtained by imposing that $D_5(\gamma)$ in Equation (33) be equal to ± 1 , can be reduced by one by dividing it for $\cos \gamma \mp 1$. The latter equation is of degree four and its solution can therefore be analytically determined, by means of Cardan method [39], although it is quite cumbersome. In practice, when the layers per cell are more than four, the solution of the equation will be performed numerically.

3.1.5. Higher Number of Layers

The above equations for K can be generalized by the formula

$$K_N = \sum_{i=1}^{N-1} \sum_{j=i+1}^N \frac{Z_i}{Z_j}, \quad (36)$$

which refers to a typical case of N layers, and includes $N(N-1)/2$ terms.

The formula for A can also be generalized to higher N . For example, with $N = 6$ the formula

$$A_6 = \sum_{i=1}^{N-3} \sum_{k=i+1}^{N-2} \sum_{j=k+1}^{N-1} \sum_{l=j+1}^N \left(\frac{Z_i Z_j}{Z_k Z_l} + \frac{Z_k Z_l}{Z_i Z_j} \right), \quad (37)$$

is obtained.

The extension to higher values of N of the dispersion relation can be obtained by straightforward generalization of the above results. For even values of N the following result is obtained

$$\cos(k_e^{(N)} a) = D_e(\gamma) = \sum_{j=0}^{N/2} a_j^{(N)} \cos^{N-2j} \gamma \sin^{2j} \gamma, \quad (38)$$

while for odd N we have

$$\cos(k_e^{(N)} a) = D_o(\gamma) = \cos \gamma \left(\sum_{j=0}^{(N-1)/2} b_j^{(N)} \cos^{N-1-2j} \gamma \sin^{2j} \gamma \right). \quad (39)$$

The coefficients $a_j^{(N)}$ and $b_j^{(N)}$ could be given explicitly as functions of the Z_j impedances, but they turn out to be cumbersome as soon as N exceeds few units (as can be guessed, e.g., from Equation (35)). Since their roles have been already seen in our previous examples, it is more convenient to use them directly in numerical form.

Without going into details we show two further cases at the plot level in Figure 8a,b, where the functions $D_o(\gamma)$, (Equation (39)), with $N = 7$, and $D_e(\gamma)$, (Equation (38)), with $N = 10$, have been used, respectively, adopting for the Z_j the numerical values shown in the figure captions. In both cases, the crossings of the ± 1 lines delimit $N - 1$ bandgaps.

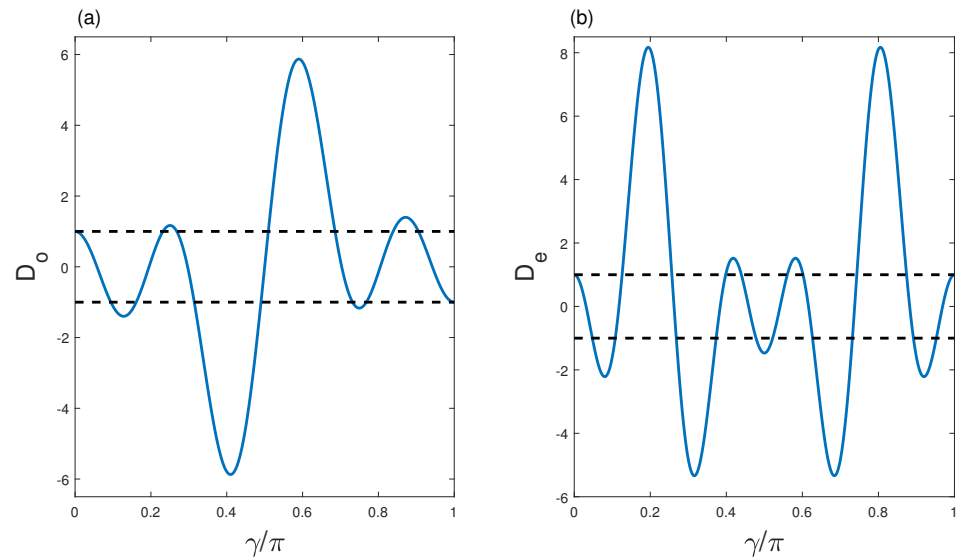


Figure 8. (a) Plot of the function $D_o(\gamma)$, (Equation (39)), in the case of seven layers per cell ($N = 7$) with impedances: (2.0, 1.4, 2.3, 2.9, 1.2, 2.2, 0.4). (b) Plot of the function $D_e(\gamma)$, (Equation (38)), in the case of ten layers per cell ($N = 10$) with impedances: (1.0, 0.2, 0.3, 1.4, 2.5, 0.6, 1.8, 2.7, 3.0, 3.5).

Elementary solutions of the equations used to determine the locations of the bandgaps exist up to the case of nine layers per cell: the equation in this case is traced back to one of degree eight that, in turn, can be recast into a fourth degree equation, presenting known analytical solutions.

3.2. Finite Crystals

In the previous section we considered an ideal crystal, hence of infinite length, for which the Floquet-Bloch [40] theorem holds true, and this allowed us to study the crystal dispersion using the properties of a single unit cell. This, in particular, showed the existence of bandgaps (or forbidden bands). Since a physical crystal is finite, we can wonder how its properties change when only a finite number M of unit cells exists. In operative terms, for a finite crystal it is possible to introduce certain (measurable) quantities, like the transmission and reflection functions, which do not have any concrete meaning for a crystal of infinite length.

We shall consider the case of one or more unit cells immersed in one and the same medium, whose impedance we denote by Z_0 . All the other impedances can be measured in units of Z_0 . The transmission function [13] only will be considered, on assuming that the system is lossless, so that the reflection function can be derived from the first.

We shall study the transmission of an incoming wave when it encounters a cascade of unit cells, starting from a single cell and moving to higher numbers.

The simplest case is that of a crystal constituted by a single unit cell, in which one layer only with impedance Z_1 exists. If more cells are cascaded, the results will be the same as those of a single cell, except for an increased length of the layer it contains. Accordingly, it is enough to consider a single cell only. The pertinent transmission function is well known [37] and its modulus is given by

$$|t(\gamma)| = \left[1 + \frac{1}{4} \left(\frac{Z_1}{Z_0} - \frac{Z_0}{Z_1} \right)^2 \sin^2 \gamma \right]^{-1/2}, \quad (40)$$

whose plot is the periodic repetition of the square root of a Lorentzian curve having $\sin \gamma$ as a variable. It is seen that the curve dynamics grows on increasing Z_1/Z_0 . Several examples are given in Figure 9, for different values of the Z_1/Z_0 ratio.

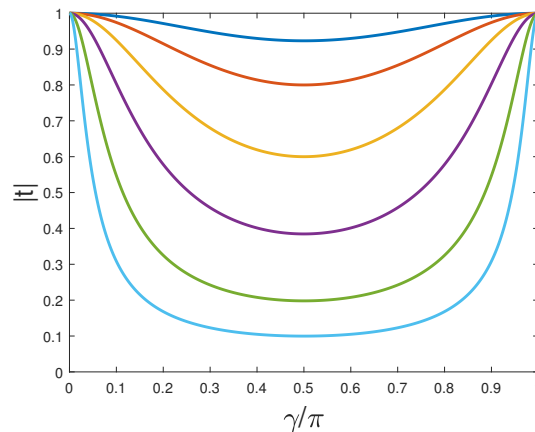


Figure 9. Plot of Equation (40) for $Z_1/Z_0 = 1.5, 2.0, 3.0, 5.0, 10, 20$, from highest to lowest curve.

In general, when the transmission function is obtained by the transfer matrix method its expression reads [13]

$$t(\gamma) = \frac{2 \exp(i\gamma)}{[T_{11}(\gamma) + T_{12}(\gamma)/Z_0 + T_{21}(\gamma)Z_0 + T_{22}(\gamma)]}, \quad (41)$$

where the $T_{ij}(\gamma)$, ($i, j = 1, 2$) are the elements of the transfer matrix that pertains to the set of cells that we are considering. When there is one unit cell only, containing a single layer, the modulus of the transmission function is, of course, given by Equation (40).

3.2.1. Two Layers per Cell

The next case to consider is that in which there is a single unit cell containing two layers with distinct impedances, say Z_1 and Z_2 . To better highlight the features of the transmission function, it is convenient to assume such impedances to be much higher than that (Z_0) of the host medium. We shall assume instead that Z_1 and Z_2 have a little difference. Generalizations of the present hypotheses will be seen later on.

The transmission function modulus for one cell containing two layers with impedances $Z_1 = 10.1$ and $Z_2 = 10.0$, on assuming $Z_0 = 1.00$, (full line in Figure 10a) is of the form already seen in Figure 9, pertaining to the single layer, where a periodic peak with period π can be seen, except that now another peak is present at $\pi/2$. (Note that one peak is divided, so to say, between 0 and π). When a second cell is added, the modulus of the new transmission function has two times more peaks (dashed plot in Figure 10a).

Passing to the case of a crystal with ten cells, the transmission function modulus of Figure 10b is obtained. Now, twenty peaks can be seen in $0, \pi$. It can be noticed that the minima of the transmission function do not depend on the number of cells. In addition, it is verified that they are only function of Z_1/Z_0 and Z_2/Z_0 . At a closer scrutiny, however, something new appears. Indeed, if we enlarge the upper part of the plot, as in Figure 11a, where only the vertical interval 0.95–1.00 is shown, we see that the maximum centered at $\pi/2$ is lower than the others. Indeed, we do not expect to find a normal mode of the structure at $\gamma = \pi/2$, which would only occur if $Z_1 = Z_2$ because of the doubled unit cell.

For a quantitative estimate, we note that the value of $|t(\pi/2)|$ can be easily evaluated in closed form for any value, say M , of the number of cells that are considered. Indeed, using Equation (9), we find

$$|t(\pi/2)| = \frac{2}{(Z_1/Z_2)^M + (Z_2/Z_1)^M}, \quad (42)$$

showing that, on increasing M , the quantity $|t(\pi/2)|$ tends to zero as $(Z_2/Z_1)^M$. This is a manifestation of the existence of a bandgap. In the case of many more cells (100 and 650 in Figure 11b, values empirically determined to illustrate the trend), the bandgap approximation becomes more and more significant, even if the limit of zero transmission will never be reached by a finite number of unit cells. Notice that the plotting interval is only $\pi/100$. The width of the bandgap obtained with 650 cells, approximately equal to 0.003π , fits well with the prediction of Equation (14).

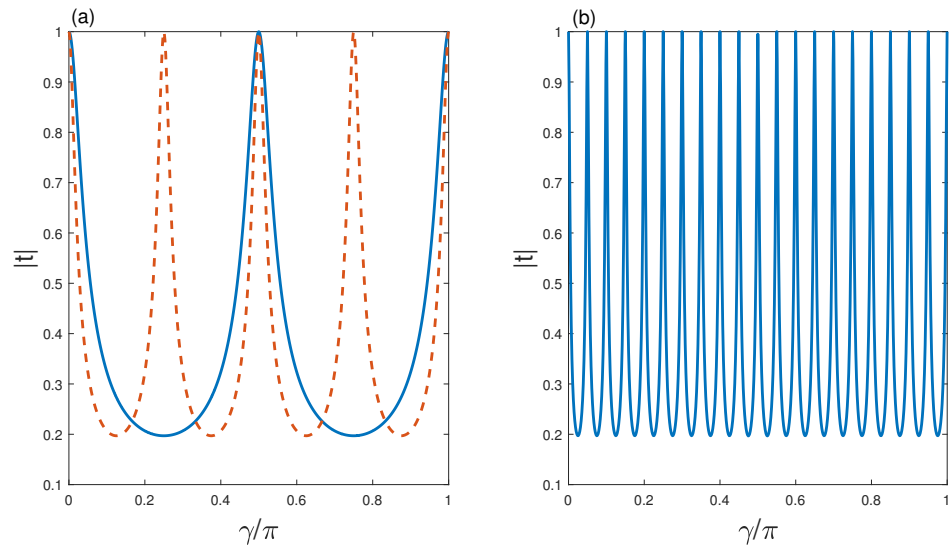


Figure 10. (a) Transmission function modulus of a finite crystal constituted by one (full line) and two (dashed line) cells with two layers per cell when $Z_0 = 1.00$, $Z_1 = 10.1$, $Z_2 = 10.0$. (b) Same as in (a) but with ten cells.

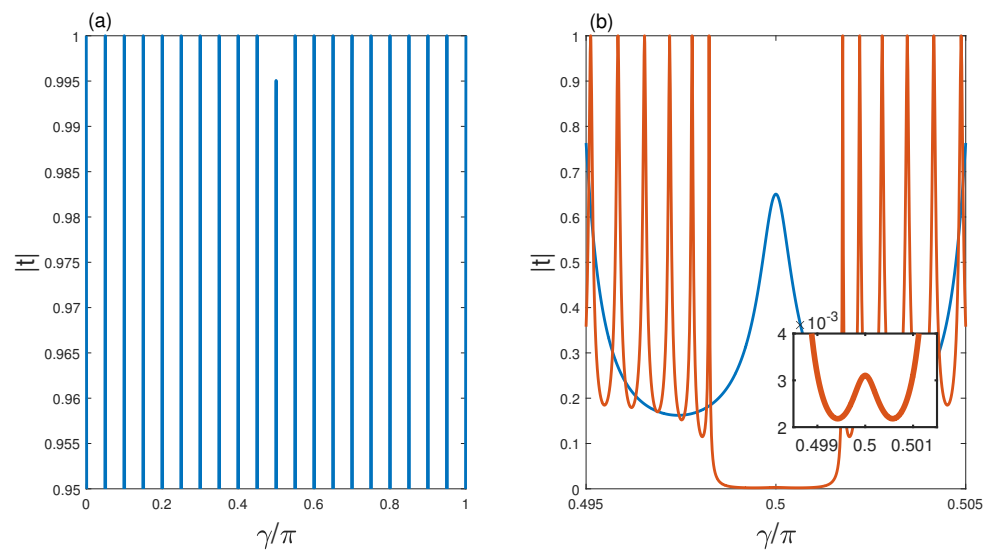


Figure 11. (a) Same as Figure 10b, except that only the vertical interval 0.95–1.00 is shown. (b) Same as Figure 10b, but with 100 cells (blue line) and 650 cells (orange line). Only a small horizontal interval enclosing $\gamma = \pi/2$ is shown. The inset shows a zoom of the low-transmission interval.

It is easily possible to determine the number M of cells needed to obtain a prescribed value of the modulus of the transmission function, say ε , at $\gamma = \pi/2$. The value of M is found to be

$$M = \left\lceil \frac{1}{\log(Z_1/Z_2)} \log \left(\frac{1 \pm \sqrt{1 - \varepsilon^2}}{\varepsilon} \right) \right\rceil, \tag{43}$$

where the symbol $\lceil \cdot \rceil$ denotes the ceiling function. In the previous expression the sign in front of the square root has to be determined so that M results in a positive value: the $+$ sign is needed if $Z_1 > Z_2$, the $-$ sign in the opposite case.

We now move to the case where the mismatch Z_1/Z_0 is small while Z_1 and Z_2 are still close. We consider again cells with two layers and let $Z_0 = 10.00$, $Z_1 = 10.05$, $Z_2 = 9.95$. The corresponding transmission function modulus, when a single two-layer cell is present (not shown), seems to be flat at the value 1, but a small decrease of the transmission can be detected at $\pi/2$. The tendency to a bandgap is made evident by increasing the number of cells, as done in Figure 12a,b where the transmission function moduli obtained with 100 and 650 cells are shown. Notice again that in the second figure the plotting interval is only $1/100$ of the Brillouin zone around its center.

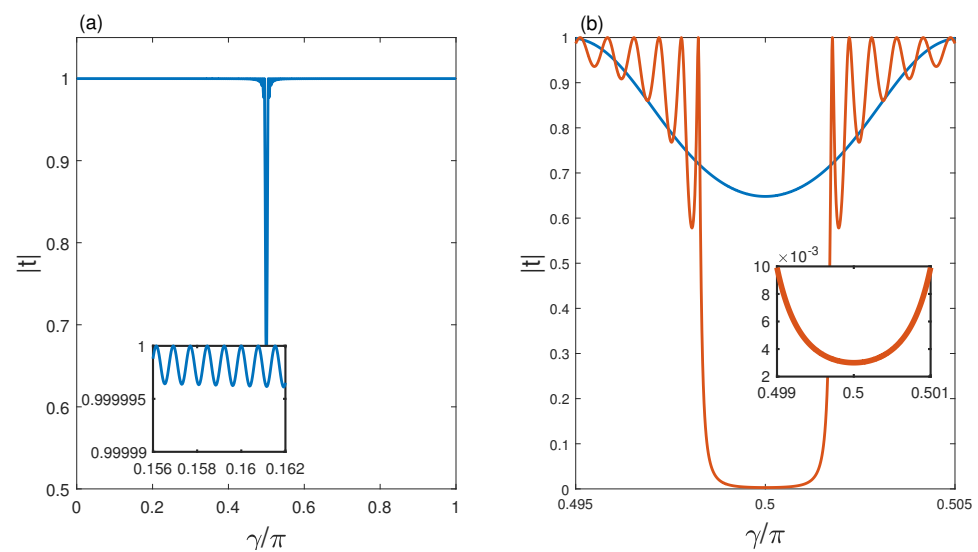


Figure 12. (a) Transmission function modulus when 100 bilayer cells are present with $Z_0 = 10.00$, $Z_1 = 10.05$, $Z_2 = 9.95$. The inset shows the very small oscillations that are present far from the center of the Brillouin zone. (b) Transmission function modulus when 100 (orange line) and 650 (blue line) bilayer cells are present. Same impedances as in (a). Only a small horizontal interval around the center of the Brillouin zone is shown. The inset shows a zoom of the low-transmission interval.

The transmission function modulus outside such an interval seems to quickly reach the value one and to stay there. Actually, with a suitably high magnification an oscillatory behavior can be seen, as shown in the inset of Figure 12a: a very small oscillation that acts on the sixth decimal digit is present.

Up to now, we assumed the layer impedances to be rather similar to one another. We have now to add something when such a hypothesis does not hold true. The essential difference with respect to the previous cases is that the asymptotic region is reached with many less unit cells. As an example, we present the case of a finite crystal with two layers per cell, 10 unit cells, and the following impedances: $Z_0 = 1.0$, $Z_1 = 10$, and $Z_2 = 20$. As seen from Figure 13, the bandgap centered at $\pi/2$ is already well defined. Compared with previous cases, the bandgap centered at $\pi/2$ is much wider, consistently with the dependence on K_2 shown in Equation (14) for the infinite crystal.

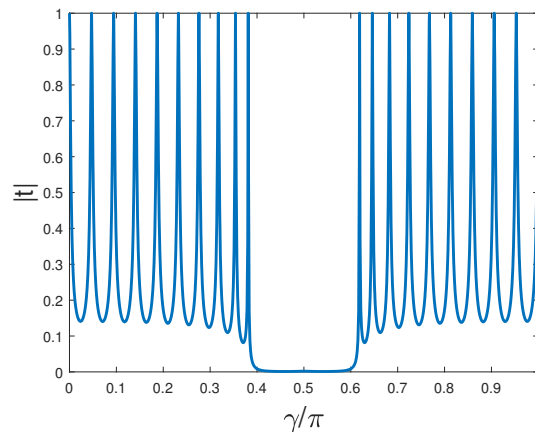


Figure 13. Birth of the bandgap with $Z_0 = 1.0$, $Z_1 = 10$, and $Z_2 = 20$, using a bi-layer finite crystal with 10 unit cells.

3.2.2. Three Layers per Cell

Cases where three layers are present in each unit cell can be treated analogously. In Figure 14a,b, obtained with three layers of comparable impedances, the birth of two bandgaps at $\pi/3$ and $2\pi/3$ is foreseen by the reduction of the transmission function peaks (discernible in Figure 14b).

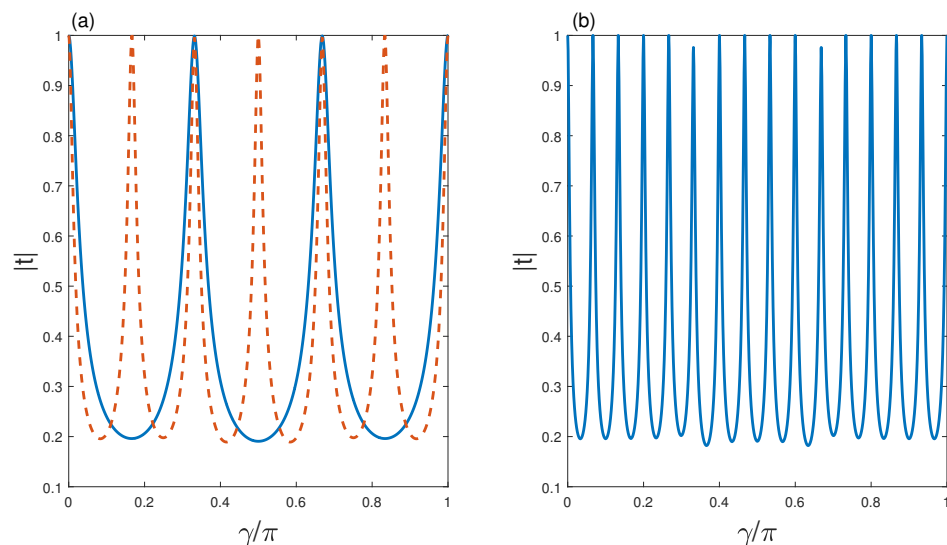


Figure 14. (a) Transmission function modulus of a finite crystal with 3 layers per cell, when one cell only is present (full line), and when two cells are present (dashed line). $Z_0 = 1.00$, $Z_1 = 10.5$, $Z_2 = 10.0$, $Z_3 = 9.90$. (b) Same as in (a) but with five cells.

In the previous section, a simple closed-form value of the transmission function at $\pi/2$ has been found in Equation (42), valid for any M in the case of two layers per cell. When three layers per cell are used, the behavior at $\pi/2$ is different for even or odd values of M . If M is equal to 1, i.e., one single cell made up of three layers, the overall transfer function at $\pi/2$ is given by

$$\begin{aligned} \mathbf{T}_{3l,1}\left(\frac{\pi}{2}\right) &= \mathbf{T}_1\left(\frac{\pi}{2}\right)\mathbf{T}_2\left(\frac{\pi}{2}\right)\mathbf{T}_3\left(\frac{\pi}{2}\right) \\ &= \begin{bmatrix} 0 & -i\frac{Z_1Z_3}{Z_2} \\ -i\frac{Z_2}{Z_1Z_3} & 0 \end{bmatrix}. \end{aligned} \quad (44)$$

When an even number $M = 2n$ of cells is used, the pertaining transfer matrix is

$$\begin{aligned} \mathbf{T}_{3l,2n}\left(\frac{\pi}{2}\right) &= \left[\mathbf{T}_1\left(\frac{\pi}{2}\right)\mathbf{T}_2\left(\frac{\pi}{2}\right)\mathbf{T}_3\left(\frac{\pi}{2}\right)\right]^{2n} \\ &= \left\{\left[\mathbf{T}_1\left(\frac{\pi}{2}\right)\mathbf{T}_2\left(\frac{\pi}{2}\right)\mathbf{T}_3\left(\frac{\pi}{2}\right)\right]^2\right\}^n = (-\mathbf{I})^n, \end{aligned} \quad (45)$$

with \mathbf{I} the identity matrix.

When, instead, the number of cells is odd, $M = 2n + 1$, we obtain

$$\begin{aligned} \mathbf{T}_{3l,2n+1}\left(\frac{\pi}{2}\right) &= \left[\mathbf{T}_1\left(\frac{\pi}{2}\right)\mathbf{T}_2\left(\frac{\pi}{2}\right)\mathbf{T}_3\left(\frac{\pi}{2}\right)\right]^{2n+1} \\ &= (-\mathbf{I})^n\mathbf{T}_{3l,1}\left(\frac{\pi}{2}\right). \end{aligned} \quad (46)$$

It follows that, for any even value of M , the modulus of the transmission function (see Equation (41)) is $|t(\pi/2)| = 1$, while for any odd value of M

$$\left|t\left(\frac{\pi}{2}\right)\right| = \frac{2}{\frac{Z_1Z_3}{Z_0Z_2} + \frac{Z_0Z_2}{Z_1Z_3}}. \quad (47)$$

In both cases, the modulus of the transmission function at $\pi/2$ does not depend on the number of cells M . The overall behavior is consistent with the fact that the value of the transmission function at $\pi/2$ is not expected to tend to zero for large M as the bandgaps that occur for the infinite crystal are symmetrically located with respect to $\pi/2$, as seen in Section 3.1.2. Figure 15a,b illustrate this point.

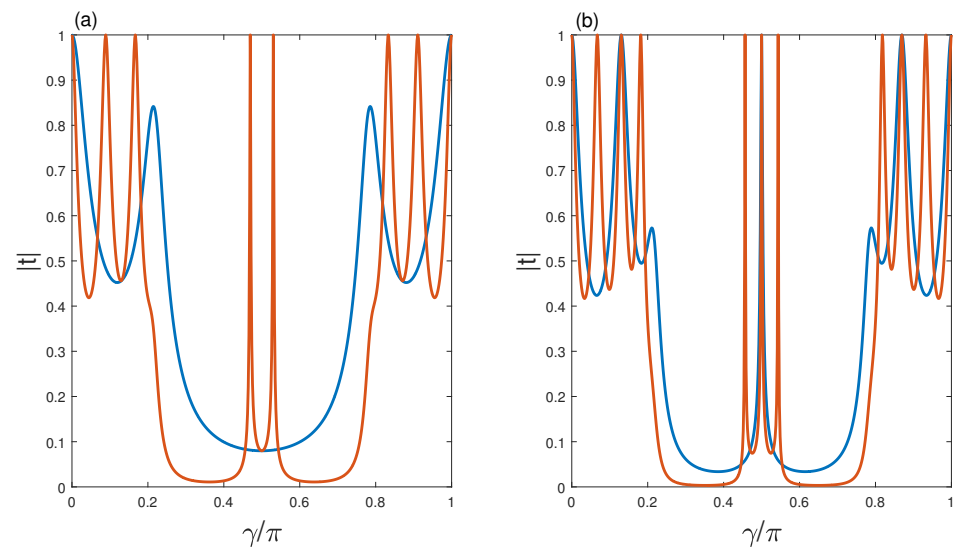


Figure 15. Transmission function modulus of a three-layer crystal with $Z_0 = 1.0$, $Z_1 = 10$, $Z_2 = 2.0$, $Z_3 = 5.0$. (a) one cell (blue line), three cells (orange line). (b) two cells (blue line), four cells (orange line).

In the case of two cells, as shown in Figure 15b, there is a single isolated central transmission peak whose width depends on the relative values of the impedances of the layers that make up the cell. Then we can consider the simpler case where only two different materials alternate, the embedding medium and another one, with impedance Z_1 . The impedances of the three layers in the unit cell are, therefore, Z_1, Z_0 and Z_1 . A structure constituted by two replicas of this unit cell is considered and its central transmission peak is plotted in Figure 16a for several values of the ratio Z_1/Z_0 . It should be noted that its width in units of π is very small. Therefore, a structure like this could be designed to realize a very narrow-band filter. Figure 16b highlights the significant dependence of the full width at half maximum (FWHM) of this peak on the ratio Z_1/Z_0 , especially for smaller values of the impedance ratio.

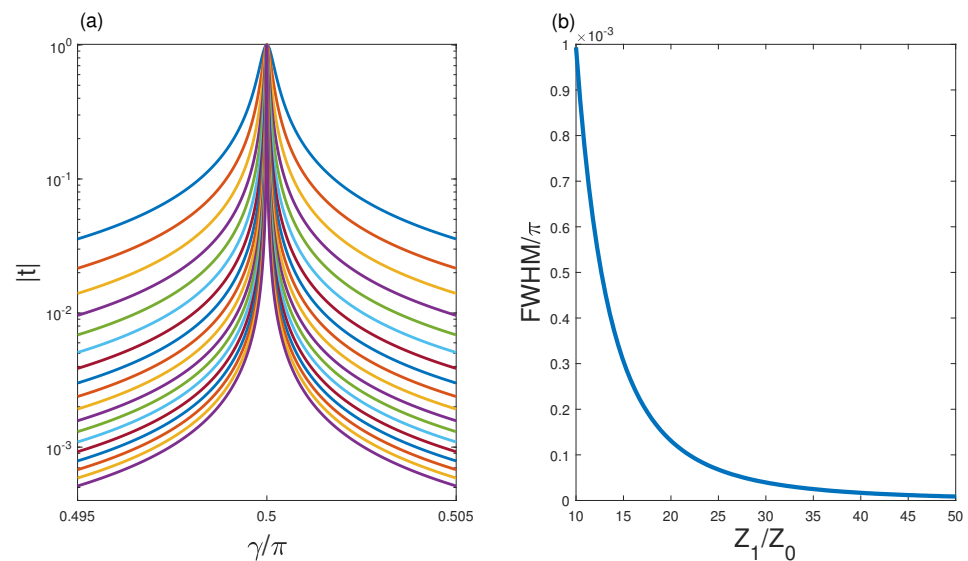


Figure 16. (a) Central transmission peak for a structure composed by two replicas of a three-layer unit cell with impedances Z_1, Z_0, Z_1 , for several values of the ratio Z_1/Z_0 (from 10, largest curve, to 50, narrowest curve); (b) FWHM of the transmission peak in (a) versus the ratio Z_1/Z_0 .

3.2.3. More Layers per Cell

For an example with a considerable number of layers, we now examine the case of a finite crystal whose cells have seven layers. The specific example we consider is performed with the same impedances used in the infinite-crystal case treated in Section 2 (Figure 8a), and is illustrated in Figure 17. The regions where the bandgaps are expected to build up, whose limits have been determined for the infinite crystal, are shown in gray in the figure.

A striking feature of the transmission function that is particularly evident in the present case is that its modulus can grow up on adding more cells. Indeed in many other cases where a transmission function is used, e.g., a set of passive cascaded transparencies, the modulus of the transmission function necessarily decreases on increasing the number of transparencies. This is because in the latter case the overall transmission function is the product of the transmission functions of the various transparencies. In our present case, instead, we have to do with the product of the transfer matrices, not of the corresponding transmission functions. One has also to bear in mind that no absorption is considered in the propagation model we are applying, and therefore the transmission function can be, at certain frequencies, strictly equal to one, even when several layers are cascaded.

Another element worth highlighting is that the rate of approaching the asymptotic regime is different for distinct bandgaps. Indeed, the narrowest bandgaps require the highest number of unit cells in order to exhibit asymptotic behavior.

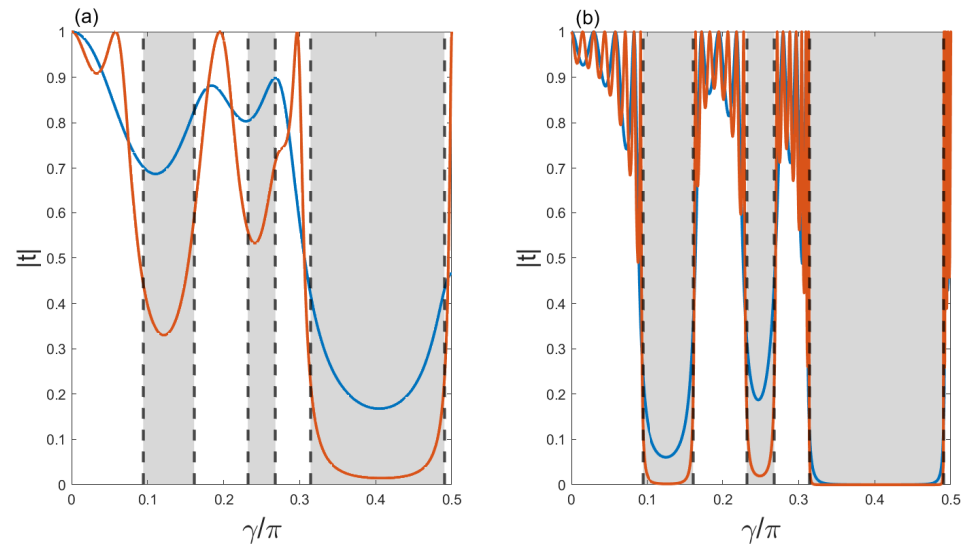


Figure 17. (a) Birth of bandgaps for a crystal with seven layers per cell, with the same impedances of the seven-layer infinite crystal in Section 2.2, in the case of one (blue line) and two (orange line) cells. Gray regions denote the band gaps. (b) Same as (a), but in the case of four (blue line) and eight (orange line) cells.

It has to be observed that, when increasing the number of cells in the finite crystal, there is a corresponding increase in the number of oscillations of the transmission function in the allowed bands. What is physically meaningful, however, is just an average value on the pseudoperiod of oscillation.

4. Discussion

For the sake of length and clarity suitable for a first approach to the problem, a few simplifying assumptions have been adopted in this work.

Only normal incidence has been considered. With oblique incidence, the required cophasality assumption would be different. This entails that the location of band gaps would be modified, with a departure from the predictions obtained for normal incidence that is a function of the incidence angle.

Furthermore, dissipation has not been included. This, formally, can be easily done by allowing a complex impedance and wavenumber. The resulting analytical treatment would be more involved, but numerical approaches can be employed.

Finally, the formalism used is strictly valid only for longitudinal waves propagating in an inviscid fluid. To a first approximation, however, the modeling can be applied also to longitudinal waves excited in homogeneous isotropic solids. More accurate modeling of the elastodynamic behavior requires an approach that is beyond the scope of this work.

Addressing some of the highlighted limitations will be the aim of further work. In addition, it will be important to understand how to exploit the cophasal assumption to guide the synthesis of acoustic structures with prescribed requirements in terms of location and widths of the bandgaps. Another point to investigate will be how the departures from the exact cophasality assumption affect the behavior of a periodic crystal and of its finite-size realizations.

For what concerns the materials that could be used to realize the cophasal layered structures, there is a wide range of choices. The parameters that control the band gap width are K_i (with i the number of layers per cell) and A_i (if $i > 3$). Both of them only depend on ratios of impedances. Assuming the longitudinal wave propagation to dominate, combinations of materials from porous (Z in the range of $10^3 - 10^4$ Rayls) to liquid-like (Z in the range of MRayls) to solid ones (Z in the range of tens of MRayls) can be used.

Within the limits of validity just outlined, we want here to stress the advantage of the approach we proposed in this paper. An example can explain it clearly. With reference to a three-layer per cell crystal, we found that an assigned dispersion law can be obtained with infinitely many different pairs of impedance elements (see Equation (19) and Figure 4), a result that couldn't possibly be reached on the basis of numerical results. The concrete importance of such a result can be appreciated by noting that, if a layer with required impedance were to be found, this could be difficult to achieve, given the finiteness of actually existing materials, while, instead, matching two layers (among infinitely many) by choosing a suitable working point along a specific contour line is much easier.

In addition, the advantage of the presented approach is to have the possibility to employ pen-and-paper formulas to address the first stage of the design of acoustic structures where the occurrence of a band gap can be easily controlled. This can prove a valuable tool also for professional users needing to address this kind of design, without requiring from the beginning the set up of numerical simulations.

5. Conclusions

We presented a study of multilayer periodic structures in which acoustic waves propagate, in the form of normally incident harmonic plane waves. In order to determine the dispersion law of an infinite structure and then the corresponding transmission function of a finite approximation of it, i.e., with a finite number of cells, we assumed working with a Goupillaud-type medium, where equally phased, or cophasal, layers occur. This means that an acoustic wave experiences the same travel time through each layer. The consequences of this assumption are very appealing because the formal simplification of the expressions that dictate the dispersion law allowed us to obtain several useful results on bandgap location and width that can be used to tailor the design of the periodic structure according to the application requirements.

For infinite crystals composed of N layers per cell, $N - 1$ bandgaps arise as a consequence of the imposed periodicity. In particular, in the case of two or three layers per cell, it has been shown that the locations and widths of the bandgaps only depend on a single mismatch parameter that combines the ratios of the impedances of the component layers. When four or five layers per cell are present, the dispersion relations and the bandgaps boundaries depend on the mismatch parameter and on an additional adimensional parameter, which is also a function of the layer impedances. It is worth stressing that in all these cases the expressions of the locations and widths of the bandgaps are determined by solving elementary second-degree equations.

For crystals with six to nine layers per cell, analytical expressions could also be determined, but they are more cumbersome and have not been explicitly reported. Nonetheless, analytical expressions can be easily derived and used in practical design.

Finite-crystal approximations of the ideally periodic structures have been then addressed. In the case of a two-layer unit cell, the value of the modulus of the transmission function at the middle of the IBZ, around which a bandgap is located for the infinite crystal, has been analytically derived. This value, monotonically decreasing with the number of cells of the finite crystal, can be taken as a design parameter to calculate the number of cells needed to achieve a prescribed value of the modulus of the transmission function at the middle of the IBZ. Also in the case of three layers per cell, the modulus of the transmission function at the center of the IBZ, which occurs inside an allowed band, has been analytically calculated. The simplest case of three-layer cell, i.e., the one characterized by the sequence of impedances Z_1, Z_0, Z_1 , being Z_0 also the impedance of the embedding medium, has been also addressed. This structure, in particular its realization with only two cells, could be used as a narrow-band filter. A further increase of the number of layers per cell has highlighted

that distinct bandgaps present different rates of approaching the asymptotic regime and that the transmission function does not necessarily decrease on adding more cells.

The main contribution of this work is the formulation of a mathematical framework that provides closed-form results useful both for the analysis and the synthesis of periodic layered structures. Even in cases where the cophasality hypothesis is only approximately met, the modeling presented in this work can prove useful as a reference case to avoid a design simply based on a trial-and-error approach.

Potential applications of the approach proposed in this work are in the design of artificial layered structures, in the acoustic or in the ultrasonic range, where the low-transmission frequency range can be easily tuned by making use of the analytic relationships developed here. In addition, it is straightforward to apply them to other wave domains that share the same mathematical framework.

Author Contributions: Conceptualization, P.G., C.G. and F.A.; methodology, P.G. and C.G.; software, C.G. and L.E.; validation, P.G., C.G. and L.E.; formal analysis, P.G. and L.E.; writing—original draft preparation, P.G. and L.E.; writing—review and editing, C.G., F.A. and R.D.L.V.; supervision, P.G., R.D.L.V. and F.A. All authors have read and agreed to the published version of the manuscript.

Funding: This research received no external funding.

Data Availability Statement: The original contributions presented in this study are included in the article. Further inquiries can be directed to the corresponding author.

Conflicts of Interest: The authors declare no conflicts of interest.

References

1. Brillouin, L. *Wave Propagation in Periodic Structures*; MacGraw-Hill: New York, NY, USA, 1946.
2. Ursin, B. Review of elastic and electromagnetic wave propagation in horizontally layered media. *Geophysics* **1983**, *48*, 1063–1081. [[CrossRef](#)]
3. Brouard, B.; Lafarge, D.; Allard, J.F. A general method of modelling sound propagation in layered media. *J. Sound Vib.* **1995**, *183*, 129–142. [[CrossRef](#)]
4. Brekhovskikh, L.M.; Godin, O.A. *Acoustics of Layered Media I: Plane and Quasi-Plane Waves*; Springer Science & Business Media: New York, NY, USA, 2012.
5. Setaki, F.; Tenpierik, M.; Turrin, M.; van Timmeren, A. Acoustic absorbers by additive manufacturing. *Build. Environ.* **2014**, *72*, 188–200. [[CrossRef](#)]
6. Fotsing, E.R.; Dubourg, A.; Ross, A.; Mardjono, J. Acoustic properties of periodic micro-structures obtained by additive manufacturing. *Appl. Acoust.* **2019**, *148*, 322–331. [[CrossRef](#)]
7. Sekar, V.; Fouladi, M.H.; Namasivayam, S.N.; Sivanesan, S. Additive Manufacturing: A Novel Method for Developing an Acoustic Panel Made of Natural Fiber-Reinforced Composites with Enhanced Mechanical and Acoustical Properties. *J. Eng.* **2019**, *2019*, 4546863. [[CrossRef](#)]
8. Shen, M.; Cao, W. Acoustic band-gap engineering using finite-size layered structures of multiple periodicity. *Appl. Phys. Lett.* **1999**, *75*, 3713–3715. [[CrossRef](#)]
9. Mangipudi, K.R.; Jooss, C.; Volkert, C.A. Achieving large acoustic and phonon band gaps in multilayered structures. *Phys. Status Solidi A* **2016**, *213*, 824–830. [[CrossRef](#)]
10. Isaac, C.W.; Pawelczyk, M.; Wrona, S. Comparative study of sound transmission losses of sandwich composite double panel walls. *Appl. Sci.* **2020**, *10*, 1543. [[CrossRef](#)]
11. Ciaburro, G.; Parente, R.; Iannace, G.; Puyana-Romero, V. Design optimization of three-layered metamaterial acoustic absorbers based on PVC reused membrane and metal washers. *Sustainability* **2022**, *14*, 4218. [[CrossRef](#)]
12. Martin, P. N masses on an infinite string and related one-dimensional scattering problems. *Wave Motion* **2014**, *51*, 296–307. [[CrossRef](#)]
13. Jiménez, N.; Umnova, O.; Groby, J.P. *Acoustic Waves in Periodic Structures, Metamaterials, and Porous Media*; Springer: Berlin/Heidelberg, Germany, 2022.
14. Sánchez-Soto, L.L.; Monzón, J.J.; Barriuso, A.G.; Cariñena, J.F. The transfer matrix: A geometrical perspective. *Phys. Rep.* **2012**, *513*, 191–227. [[CrossRef](#)]

15. Adler, E.L. Matrix methods applied to acoustic waves in multilayers. *IEEE Trans. Ultrason. Ferroelectr. Freq. Control* **1990**, *37*, 485–490. [[CrossRef](#)] [[PubMed](#)]
16. Lee, C.M.; Xu, Y. A modified transfer matrix method for prediction of transmission loss of multilayer acoustic materials. *J. Sound Vib.* **2009**, *326*, 290–301. [[CrossRef](#)]
17. Li, J.; Zhu, X.; Shen, C.; Peng, X.; Cummer, S.A. Transfer matrix method for the analysis of space-time-modulated media and systems. *Phys. Rev. B* **2019**, *100*, 144311. [[CrossRef](#)]
18. Mackay, T.G.; Lakhtakia, A. *The Transfer-Matrix Method in Electromagnetics and Optics*; Springer Nature: Berlin, Germany, 2022.
19. Fayon, L.; Knapmeyer-Endrun, B.; Lognonné, P.; Bierwirth, M.; Kramer, A.; Delage, P.; Karakostas, F.; Kedar, S.; Murdoch, N.; Garcia, R.F.; et al. A numerical model of the SEIS leveling system transfer matrix and resonances: Application to SEIS rotational seismology and dynamic ground interaction. *Space Sci. Rev.* **2018**, *214*, 119. [[CrossRef](#)]
20. Liang, J.; Wu, M.; Ba, Z.; Lee, V.W. Transfer matrix solution to free-field response of a multi-layered transversely isotropic poroelastic half-plane. *Soil Dyn. Earthq. Eng.* **2020**, *134*, 106168. [[CrossRef](#)]
21. Biswas, D.; Kumar, V. Improved transfer matrix methods for calculating quantum transmission coefficient. *Phys. Rev. E* **2014**, *90*, 013301. [[CrossRef](#)] [[PubMed](#)]
22. Ibarra-Reyes, M.; Pérez-Álvarez, R.; Rodríguez-Vargas, I. Transfer matrix in 1D Dirac-like problems. *J. Phys. Condens. Matter* **2023**, *35*, 395301. [[CrossRef](#)]
23. Lauriks, W.; Mees, P.; Allard, J. The acoustic transmission through layered systems. *J. Sound Vib.* **1992**, *155*, 125–132. [[CrossRef](#)]
24. Song, B.H.; Bolton, J.S. A transfer-matrix approach for estimating the characteristic impedance and wave numbers of limp and rigid porous materials. *J. Acoust. Soc. Am.* **2000**, *107*, 1131–1152. [[CrossRef](#)]
25. Dell, A.; Krynkina, A.; Horoshenkov, K.V. The use of the transfer matrix method to predict the effective fluid properties of acoustical systems. *Appl. Acoust.* **2021**, *182*, 108259. [[CrossRef](#)]
26. Sigalas, M.M. Elastic and acoustic wave band structure. *J. Sound Vib.* **1992**, *158*, 377–382. [[CrossRef](#)]
27. Khelif, A.; Adibi, A. *Phononic Crystals*; Springer: Berlin/Heidelberg, Germany, 2015.
28. Stoica, L.G.; Marco, A.D.; Gori, P. Metamodeling and optimisation of a sonic crystal-based noise attenuation device. In Proceedings of the INTER-NOISE and NOISE-CON Congress and Conference Proceedings, Seoul, Republic of Korea, 23–26 August 2020; Volume 261, pp. 256–266.
29. Vasileiadis, T.; Varghese, J.; Babacic, V.; Gomis-Bresco, J.; Navarro Urrios, D.; Graczykowski, B. Progress and perspectives on phononic crystals. *J. Appl. Phys.* **2021**, *129*, 160901. [[CrossRef](#)]
30. D’Orazio, T.; Asdrubali, F.; Godinho, L.; Veloso, M.; Amado-Mendes, P. Experimental and numerical analysis of wooden sonic crystals applied as noise barriers. *Environments* **2023**, *10*, 116. [[CrossRef](#)]
31. Goupillaud, P.L. An approach to inverse filtering of near-surface layer effects from seismic records. *Geophysics* **1961**, *26*, 754–760. [[CrossRef](#)]
32. Velo, A.P.; Gazonas, G.A. Optimal design of a two-layered elastic strip subjected to transient loading. *Int. J. Solids Struct.* **2003**, *40*, 6417–6428. [[CrossRef](#)]
33. Gazonas, G.; Velo, A. Analytical solutions for the resonance response of Goupillaud-type elastic media using z-transform methods. *Wave Motion* **2012**, *49*, 135–151. [[CrossRef](#)]
34. Farmer, C.; Ockendon, H.; Ockendon, J. One-dimensional acoustic waves in air/water mixtures. *Wave Motion* **2021**, *106*, 102798. [[CrossRef](#)]
35. Asdrubali, F.; Schiavoni, S.; Horoshenkov, K. A review of sustainable materials for acoustic applications. *Build. Acoust.* **2012**, *19*, 283–311. [[CrossRef](#)]
36. Gori, P.; Guattari, C.; Asdrubali, F.; de Lieto Vollaro, R.; Monti, A.; Ramaccia, D.; Bilotti, F.; Toscano, A. Sustainable acoustic metasurfaces for sound control. *Sustainability* **2016**, *8*, 107. [[CrossRef](#)]
37. Kinsler, L.E.; Frey, A.R.; Coppens, A.B.; Sanders, J.V. *Fundamentals of Acoustics*; Wiley: New York, NY, USA, 2000.
38. Abramowitz, M.; Stegun, I.A. *Handbook of Mathematical Functions with Formulas, Graphs, and Mathematical Tables*; Dover: New York, NY, USA, 1972.
39. Hardy, G.H. *A Course of Pure Mathematics*; Cambridge University Press: Cambridge, UK, 2008.
40. Grosso, G.; Parravicini, G.P. *Solid State Physics*; Academic Press: Cambridge, MA, USA; Elsevier: Amsterdam, The Netherlands, 2014.

Disclaimer/Publisher’s Note: The statements, opinions and data contained in all publications are solely those of the individual author(s) and contributor(s) and not of MDPI and/or the editor(s). MDPI and/or the editor(s) disclaim responsibility for any injury to people or property resulting from any ideas, methods, instructions or products referred to in the content.